RSC Advances

ROYAL SOCIETY OF CHEMISTRY

www.rsc.org/advances

Structure-Color Mechanism of Iridescent Cellulose Nanocrystal Films

Dagang Liu,* *Shuo Wang*, *Zhongshi Ma*, *Donglin Tian*, *Mingyue Gu*, *Fengyin Lin*

Department of Chemistry, Nanjing University of Information Science and Technology, Nanjing, 210044

AUTHOR INFORMATION:

Corresponding author:

*Tel. & Fax: +86 2558731090, E-mail address: dagangliu@gmail.com or dagang@nuist.edu.cn (D. Liu)

ABSTRACT:

Chirality and repulsion interaction among sulfate cellulose nanocrystals (CNCs) have vital impacts on the formation of cholesteric liquid crystal (CLC) phase in the suspension or solidified film. In this work, a facile sonication treatment was applied to change the structure and repulsion interaction of CNCs and consequently tune the chiroptical properties of the resultant films. Results show that increasing sonication energy by improving input power or prolonging aging time caused the reduction of particle size, surface charge density, thereby increasing the cholesteric pitch and red-shifting the reflective wavelength of the iridescent films. The optical properties of the film followed the regulation of Bragg reflection and thin-film interference. However, over-energy input would cause multi-dispersion of CNCs according to the level of the surface charge density, thus leading to formation of polydomain CLC instead of planar CLC due to multi-distributed intra-axial drive forces. Hence, a schematic model was built up to describe the structure transition as well as the color variation and to make a connection between the mesoscopic behavior of CNCs and the microscopic interactions of electrostatic repulsion, hydrogen bonding affinity and chirality. Hence, we provided some meaningful information on building up hierarchical organization assembled from charged rigid biological rods, and help to recognize the structure-color mechanism of solidified films of polysaccharide nanocrystals.

KEYWORDS: Cellulose nanocrystal, cholesteric liquid crystal,structure, color, sonication

INTRODUCTION

Cellulose nanocrystals have attracted plenty of attentions because of their unique properties such as high stiffness and strength, high specific surface area, low coefficient of thermal expansion, optical transparency and self-assembly behavior. The low cost, renewability and recyclability, and chemical reactivity allowing its chemical and physical properties to be tailored make CNC attractive for various applications.[1] CNCs are typically extracted from cellulosic biomass using strong acid hydrolysis,[2] strong oxidation,[3] or ionic liquid.[4] Acid hydrolysis of cellulose is a well-known process of a preferential digestion of the amorphous domains and cleavage of the nanofibril bundles therefore breaking down the hierarchical structure of the raw materials into crystalline nanocrystals. Strong acids such as sulfuric acid [5] or hydrochloric acid [6] are generally used; however, hydrochloric acid CNCs have minimal surface charge and limited aqueous dispersibility, whereas sulfuric acid CNCs provide highly stable aqueous suspensions due to the esterification of surface hydroxyl groups resulting in negative charged sulfate groups.[7-9] When the homogeneous suspensions of sulfate CNCs were concentrated, nematic liquid crystal or CLC was formed after a slowing self-assembling process.[10,11] Aqueous suspension of sulfate CNCs is one kind of lyotropic liquid crystal. Another amazing property is when aqueous CNC suspension was evaporated, the chiral nematic phase was retained in the produced solid semitranslucent CNC films. CNC rods were parallelly aligned to each other and to the plane of layers, each layer being rotated slightly with respect to the layers above or below it, thereby producing helical pseudo-layers. Inspired from

fascinating chiroptical properties of CNC mesogen, the thin coatings, pigments, printing ink, and colorful films with tunable optical properties were designed,[12] and porous chiral photonic crystal was also fabricated by using CNCs as templates for deposition of inorganic nanoparticles.[13,14] Researches in CNC mesogen spontaneously arising from aqueous suspension have attracted significant interests and become a novel scientific topic of cellulose. After all, chirality and nematic phase are vital to optically functionalize CNCs based nanomaterials or templated phonotic crystals.

Beside acidic hydrolysis and oxidation, mechanical treatments, such as sonication[15] and homogenization[16-19] are commonly used to desintergrate and disperse polysaccharide nanocrystals in suspensions, e.g., sonication was thought to break up CNCs side-by-side,caused a decrease of viscosity,[9] and controlled red-shift color for CNC films by increasing input sonication energy.[20]

The cholesteric characters were described to be dependent on polydispersity, physical dimension, surface charge, and the ionic strength of the CNC particles.[16] In previous reports,[7] it was thought that the smaller average length of CNC rods would lead to a smaller pitch. However, this turns out not to be true in the case of sonication treated CNCs since the smaller sonicated particle size would lead to a larger pitch. Furthermore, based on our research experiments, CNC films processed by sonication didn't show so uniform color as those fresh-prepared films. As far as we know, the liquid crystal properties of CNC suspension had been investigated detailed,[6,7,9-12] but the color mechanisms of the CNC film are still vague. In this work, we investigated the optical properties of CNC films through turning structure and properties of CNCs

by inputting different levels of sonication energy. We hope to discover the mystery of color and establish the structure-color mechanism so that it can be applied for many other natural polymeric nanocrystalline optical materials.

EXPERIMENTAL SECTION

Materials. Microcrystalline cellulose powder (MCC, column chromatography) and sulfuric acid were purchased from Sinopharm Chemical Reagent Co., Ltd, Shanghai, China. Regenerated cellulose dialysis tubing having a molecular weight cutoff of 8,000-10,000 was supplied by Nanjing Wanqing Chemical Glassware Instrument Co., China.

Preparation of CNC suspension and film. Aqueous CNC suspensions were prepared from MCC by sulfuric acid (64%) hydrolysis at 50 ^{o}C for 2 h, and then five folds dilution with water was applied to stop the hydrolysis reaction. The diluted suspension was poured into dialysis tubing and dialyzed against deionized water for several days until the pH value at around 5.0. The freshly prepared CNC suspension had a solid content around 0.5 wt%. Mechanical sonication was performed on an ultrasonic processor (Sonics Vibra-Cell 1200 W, 19-21 kHz, HN98-IIID, Shanghai, China) with a 20 mm diameter probe and a 25% ultrasonic power ratio. Typically, 50 mL of a 0.5 wt% CNC suspension was placed in a 100 mL beaker and sonicated at 300 W. Ultrasonic disruptors were typically operated in a pulsed mode, in which the duration of on and off intervals were regulated at 10 and 20 s, respectively. In this work the sonications were carried out in an ice bath for preventing desulfation on the

surface of the nanocrystallites caused by heating of the suspension, and prolonged for 10, 20, 30, 40, 50, 60 and 70 min, respectively.

Aliquots of 0.5 wt% CNC suspension (50 mL) were sonicated with increasing energy inputs and allowed to be stable in sealed plastic box ($3.9 \times 3.9 \times 4.7$ cm^3) over a period of 72 h at ambient conditions. Then the treated suspension in the open plastic box was slowly and undisturbedly evaporated to obtain solidified CNC films in an oven at 30 ºC. All photographs of CNC films were taken normal to the films, which were placed against a black background in order to acquire the reflected iridescence under diffuse incident light.

Characterization. Zeta potential, polydispersity index (PDI), and Z-average size were measured using a Zetasizer Nano ZS90 (Malvern Instruments, U.K.). CNC suspension was performed in folded capillary cells to measure zeta potential values which were calculated using the Smoluchowski equation. Surface charge density of CNCs was determined by conductimetric titration. Approximate 1 g of a 5 wt% CNC suspension was transferred to a three-necked round bottom flask followed by addition of 200 mL of deionized water and 4 mL of 0.1 N HCl which assured an excess of H^+ in the suspension. The acid suspension was titrated with 0.01 N NaOH.

Several drops of the diluted suspension (0.1 wt%) were spin-coated onto silicon wafer chips freshly cleaned using a modified RCA protocol. At first, the chips were immersed in a solution of NH_4OH: H_2O_2: H_2O (1 : 1 : 5) at 80 ^oC for 5 min, and then rinsed repeatedly with water and immersed in a solution of HCl: H_2O_2: H_2O (1 : 1 : 5) at 80 ^oC for 5 min. Finally, the chips were dried under a N_2 stream. AFM

imaging of CNC was performed with an Asylum Research MFP-3D atomic force microscope (Santa Barbara, CA). Samples on the chips were scanned in a AC tapping mode with Tap 300 standard silicon probes (tip radius < 10 nm, spring constant at 37 N/m, resonant frequency at 300 kHz) (Budget Sensor, USA) under a 1 Hz scan rate and 1024 pixels × 1024 pixels image resolution. Polarized optical microscope (POM) observation equipped with a Nikon (Tokyo, Japan) MDA502AA E400 was used to determine the cholesteric pitch of the liquid crystalline phase in the CNC films which were placed directly on slide-glasses. Scanning electron microscopy (SEM) was performed using a Hitachi S-3600N VP SEM (Hitaschi, Japan) to investigate the morphology of the liquid crystal film. The cross-section of CNC film was coated with gold for SEM observation at 20 kV.

UV-Vis spectra were recorded on a Perkin-Elmer ultraviolet-visible spectrometer (Lambda 3B model). The optical reflectance of the sample films was measured over the wavelength region from 200 to 800 nm under 90 º incident illuminations.

RESULTS AND DISCUSSION

Structure and properties of CNCs. Z-average size, PDI, Zeta-potential, and surface charge density of CNCs measured by using Zeta-sizer are presented in Table 1. The freshly prepared CNC in this work had an Z-average size of about 176 nm, while the particle size of CNC sonicated only for 10 min was greatly reduced to 95 nm, and then the down-size effects was slowed down and tended to reach an equilibrium after treating for 50-70 min. Effect of sonication treatment on particle size and morphology

was also investigated by using AFM. As shown in Figure 1, the fresh-prepared CNCs and sonication treated CNCs in an ice bath for 70 min have a shape of needle with mean length of 159 and 81 nm, and mean diameter of 50 and 28 nm, respectively. It is interesting that the Z-average size of CNCs determined by Zeta-sizer considerably accorded with the length of nanocrystals measured by AFM. Sonication treatments markedly shortened the mean particle length and width. This may be due to the fact that CNCs, bearing defects or cracks produced by sulfate hydrolysis, were further attacked by powerful sonication and broken into down-scaled nanocrystals. As an indicator of electrostatic repulsion, surface charge density was reduced from 0.67 e/nm^2 of untreated CNCs to 0.37 e/nm^2 of CNCs treated for 70 min, owing to the increase of total surface area of particles.

The pronounced zeta potential values of freshly prepared CNCs and sonication treated CNCs were over -50 mV and showed no distinguished difference as listed in Table 1. Zeta potential was thought as an important parameter of suspended particles as it could influence both particle stability as well as particle mucoadhesion.[21] In the case of sonication treated CNCs, the absolute value of zeta potential was still at around -60 mV, indicating that the surface charge was strong enough to producing repellent interactions among nanocrystals, thus leading to a good dispersion in the suspension.[22] Furthermore, as shown in Figure 1b, either large or small nanocrystals exhibited in the sonication treated suspension, that's why size distribution was not narrowed but widened as indicated by PDI. Therefore, bath sonication drove CNCs to be well dispersed, but endowed nanocrystals with less uniformly distributed particle

size and lower surface charge density than untreated ones.

Structural color varied with processing temperature. Figure 2 shows the POM micrographs of CNC films dried at the temperature of 30 (a), 45 (b), 50 (c), and 70 ^{o}C (d), respectively. A perfect planar texture in Figure 2a indicated perfect cholesteric LC characters of the free-standing film dried at 30 ^{o}C. Although planar texture was also observed in Figure 2b, the planar mesophases were not continuous as a result of existing defects. When the casting temperature was at 50 ^{o}C, the phase without any fingerprint textures shifted to nematic mesogen as shown in Figure 2c. With a further increase of the casting temperature to 70 ^{o}C, the LC phase absolutely disappeared and the color of the film faded away (Figure 2d). In brief, with the increase of processing temperature, the liquid crystal structure of CNC films shifted from cholesteric phase, to nematic phase, and till to no LC phase at all. It is well known that sulfuric acid treated CNCs are normally associated with covalently-bound surface sulfate ester groups (typically 0.5-2%). These functional groups play an important role in forming long range ordered chiral liquid crystals, which is also true for many other cellulose derivatives bearing ethyl, hydroxypropyl, acetyl, and other groups. However, the sulfuric acid treated CNCs are sensitive to heat. At temperatures above 40-45 ^{o}C, the nanocrystals underwent slow desulfation; at 70 ^{o}C, the helical and chiral LC domains of CNCs were severely destroyed because of deeply desulfation would lead to negative charged sulfate groups dissociated from the surface of CNCs.[23,24] On the other hand, the level of order of nematic LC was related to the evaporation ratio of water from suspension because slow drying at a relative low temperature would be

beneficial for organization of CNCs into perfect cholesteric patterns, otherwise defects existed in the mesophases of fast drying samples. In this work, we preferred the temperature at 30 ^{o}C as an optimum evaporation condition for casting CNC films.

Structural color of CNC films with varied thickness. Figure 3 presents the reflection spectra of the CNC films with thickness increasing from 42, to 63, 82, and to 96 μm, respectively. It is worth noting that with increasing thickness of films (or number of layers), the peak reflectivity rather than wavelength at maximum peak increased rapidly, meanwhile the bandwidth decreased gradually. The optical characteristic of CNC chiral nematic liquid film was thought as multilayer interference, which is qualitatively understood in terms that many thin layers piles periodically.[25] When light is incident on a film, the light passes through air (refractive index, n = 1.0) → CNC (n = 1.5) → air (n = 1.0) as shown in the inset of Figure 3. Multi-layered thin film interference was applicable for reflection of chiral nematic CNC films, and the bandwidth in this case can be estimated from the difference of the wavelengths at the minimum reflectivity in the nearest oscillations. Supposing that these wavelengths reflected from (N + 1) interfaces, the interfere destructively was expressed as follows: [26]

$$2\,\hat{d} = [m \pm 1/(N+1)]\lambda \qquad (1)$$

where $\hat{d}$ is the optical path length of one layer and m is an integer, which is obtained under the assumption of only one-time reflection at each interface. According to equation established by Kinoshita,[26] the bandwidth was estimated as

follows:

$$\Delta\lambda = \frac{\lambda_+ - \lambda_-}{2} = 4(N+1)\bar{d}/[2\{m^2(N+1)^2 - 1\}] \approx 2\bar{d}/(m^2 N) \qquad (2)$$

For large N the bandwidth is inversely proportional to the number of layers. Therefore, it is necessary to pile up nematic layers to obtain high reflectivity for CNC multilayer having small refractive-index difference, which inevitably decreases the bandwidth. To reach maximum reflectivity, CNC film with thickness of 96 μm was selected as target for color-structure observations in this work.

Relationship between color and structure of sonication treated CNC film. Figure 4 shows photographs of CNC films cast from suspensions sonicated for 0, 10, 20, 30, 40, and 50 min, respectively. The films exhibit reflected iridescence in naked viewing under diffuse incident light, and the color shifted from blue to red with increasing sonication time. However, after 30 min, the color of the solidified film didn't appear as uniform as the previous one, and especially the central zone of the films sonication treated over 50 min became bleak and broad. The corresponding UV-vis reflection spectra of CNC films at 90º incident are shown in Figure 5. With extended sonication time from 0 to 70 min, the wavelengths at the maximum reflectivity of the films red-shifted from 328 to 671 nm, meanwhile the bandwidth of reflection became broaden. It is interesting that with prolongation of sonication time from 0 to 30 min, the maximum reflectivity gradually increased, but then decreased after 30 min until the reflection peak became vague for the films with sonication for 60 or 70 min. It is indicated that in this work proper sonication (300 W, 30-40 min)

was beneficial for producing uniform, bright color, whereas ultrahigh sonication energy input (high sonication power and prolonged sonication time) would take counterproductive effects.

POM micrographs of iridescent films prepared at various time levels of sonication are shown in Figure 6. Under a polarized light, free-standing films exhibit a typical planar cholesteric texture and reflective color shifted from violet (a), blue (b), cyan (c), green (d), yellow (e), orange (f), fuchsine (g), to kermesinus (h) with the prolongation of sonication. The corresponding half cholesteric pitch, defined as the distance required for CNC rods to make a 180^{o} rotation, which is simply the distance between two neighboring planar texture, dramatically increased from 0.554, 0.756, 0.877, 0.965, 1.010, 1.068, 1.205, to 1.26 μm as summarized in table 1. The liquid crystal film self-assembled from smaller crystals presents larger pitches as observed by POM.

Supposing that the observed pitch is uniformly distributed birefringent CNC film, the reflection followed Bragg's law:[27]

$$\lambda = (n_{\parallel} - n_{\perp}) P \sin\theta \qquad (3)$$

where P is the pitch of CLCs, $n_{\parallel}$ is the refractive index of light polarized parallel (extraordinary) to the optical axis and $n_{\perp}$ is for polarizations perpendicular (ordinary) to the optical axis, and θ is the angle of incidence. The refractive index is a function of the molecular composition, orientation and packing within a liquid crystal. In a cholesteric mesogen, the refractive index difference ($n_{\parallel} - n_{\perp}$) leads to the birefringence. Figure 7 demonstrates the maximum reflection wavelength as a function of cholesteric pitch of the CNC films at 90º incident angle. The result shows

that there is a linear relationship between the maximum reflection wavelength and cholesteric pitch. The value of $n_{\parallel} - n_{\perp}$ measured from the slope was 0.29, which is higher than reported value of 0.05 for the cholesteric CNC colloidal suspension.[28] It is worth noting that the curve of CNC film treated by prolonged sonication over 30 min deviated from its linear route because the Bragg reflection only accounts for the optical properties of planar cholesterics consisting of a large number of birefringent layers. In this case, $n_{\parallel} - n_{\perp}$ exhibited a decreasing trend because polydomain mesophases were observed in those over-sonicated CNC films as discussed in 3.5. Whatever, the structure-color of CNC film with planar mesophases is originated from thin-film interference and Bragg reflection.

Polydomain mesophases of CNC films. It is well known that high applied power or long treatment time would deliver high input sonication energy. Figure 8 presents the reflective spectra of CNC films produced under the sonication of 520 W for 10, 30, 120 min, respectively. The maximum reflective wavelength was red-shifted and the bandwidth was broadened, thereby the reflectivity was obviously elevated. Under a relatively high sonication power (520 W) the color of the film red-shifted in a shorter soncation time than that under low power (300 W). However, we found that under treatment of 520 W for 30 min, the resultant solid film was not uniform and the centre of the film appeared faint; and film treated by over-energy input (520 W for 120 min) appeared smooth, transparent, and colorless, as shown in the inset of Fig 8. Therefore, it is essential to control ultrasonic power and aging time to receive red-shifted iridescent film.

Figure 9 presents POM micrographs of the gloomy regions of the film produced under the sonication at 520 W for 10, 60, 120, and 150 min, respectively. Interestingly, the fingerprint region in Figure 9a-d was composed of focal conic texture with a random distribution of helical axes. The amount of polydomains with the interval distance (P/2) varying from 0.70 to 2.08 μm in Figure 9d was obviously more than those in Figure 9b. This is an evidence to address the nonlinear relationship between pitch-wavelength as shown in Figure 7 while socination time was over 30 min. Owing to ultrahigh energy input, the cholesteric mesophases became very weak (Figure 9e) and the birefringence with fingerprint texture intermittently exhibited in the transparent CNC films (Figure 9f). And also the incident light was weakly and randomly reflected and scattered in all directions, thus leading to the low reflectivity, broadened bandwidth, mixed color, and even no iridescence of the film.

Mechanism of structure-color correlation. Figure 10 shows SEM micrographs of fracture surface of CNC films which were cast from the suspension sonicated for 0, 10, 30, 50, 60, 70 min, respectively. The CNC films in Fig 10a-d exhibit fingerprint lines with regular adjacent space of about 1-2 μm at an oblique angle. Obviously, the cholesteric axis was perpendicular to the film surface and parallel to the lines. Inset picture of Figure 10b is a higher magnification image of the layered structure, in which the adjacent layer distance agreed with the P/2 value from optical microscopy. A striking feature of continuous “hill” and “hole” pattern resulted from a spontaneous twist deformation of the left-handed helicoidal hierarchy which have been described in previous work.[25] Interestingly, when ultrasonic treatment was over 10 min, the

perfect patterns was not shown on the fracture surface any more, and even disappeared in Figure 10e-f, indicating that the transition from the perfect and unique-orientated planar phase to polydomain mesophase as evidenced in Figure 9.

A great number of plant cell walls are composed of cellulose microfibrils associated with matrix components of xylan, and are typically designed as a helicoidal pattern that is analogous to a cholesteric order.[29-31] Cellulose chain in ramie has a formal geometric characteristics of a helical form with seven cellobiose residues per turn, radius r = 1.5830 Å, and angle of helix 7°51′.[32,33] Similar to many other biological macromolecules, cellulose and its derivatives have been reported to have chiroptical properties in solution or in bulk because cellulose backbone is chiral. However, strong hydrogen bonding originated from -OH groups hanging on cellulose chains are easily formed to make molecules aggregated. This is why HCl hydrolyzed CNCs didn't show liquid crystal phases in aqueous suspension. Therefore, it is crucial to create a way of weakening the hydrogen bonding attraction as well as strengthening the repulsion. As far as we know, several effective methods were adopted to obtain cellulosic CLC. The first one is to screen out the affinity by changing the polarity of solvent; the second way is to block hydrogen bonds by increasing the hydrophobicity through grafting or derivation, e.g., hydroxypropyl cellulose, ethyl cellulose, etc. The pitch height was found to increase significantly with a reduction of the substitution degree for butyric esters of (2-hydroxypropyl) cellulose, ethyl-cyanoethyl cellulose, e.g., increase of DS from 1.90-2.96 caused a significant decrease of P from 641 to 275 nm.[34] The third approach is to keep the handness of cellulose but improve the

electrostatic repulsion by increasing surface charges, e.g., sodium cellulose sulfate, sulfate hydrolyzed CNCs, etc. According to Chilaya,[35] the cholesteric pitch and the twist angle θ is related by:

$$P = 2\pi \frac{r}{\theta} \quad (4)$$

Where θ is angle between neighboring nematic planes, and r is unknown parameter indicating separation between adjacent nematic planes. Obviously, increasing layer distance or weakening the twisting force or angle is beneficial for increasing the pitch. Therefore, as mentioned above, increasing the DS of cellulose derivatives, weakening the hydrogen bonding by solvents, or properly increasing ionic strength by introduction of salts will increase the twisting angle θ, thereby reducing the pitch value.

In this work, the sulfuric acid CNC have negatively charged surfaces due to the esterification of hydroxyl groups by sulfate ions, leading to stable nanocrystal aqueous suspensions. With increasing sonication energy, CNCs were broken into smaller sized nanocrystals by the mechanical sonication disruption, thus increasing the total number as well as the specific surface area of particles. However, sonication did not affect the total surface charges which were determined by chemical hydrolysis of sulfation. This means that surface charge density of small nanocrystals was effectively reduced. As shown in Scheme 1, under low energy input of sonication, the repulsion between particles was reduced and intra-axial force at constant interaxial spacing decreased, consequently leading to the reduction of twisting angle θ. Meanwhile, the increased nanocrystals spontaneously entered into macroscopic

mesogens, thereby increasing the number of nematic layers. Hence, the pitch of the sonicated CNC mesogen increased and the maximum reflective wavelength red-shifted. However in the case of fresh-prepared CNCs,[7] the small-sized crystals, which had suffered severe hydrolysis, such as, long hydrolysis time, high acidic concentration, obviously had higher surface charge density than those large-sized CNCs, accordingly leading to a smaller pitch. That's why it is polar opposite of the CLC assembled from small-sized CNCs in this work. However, under high energy input of sonication, size or charge polydispersed nanocrystals might join in different macroscopic mesogens according to level of intra-axial force, thereby slowly self-assembling into polydomain mesophases with widely-distributed chiral pitches. Sonication would further force those nanocrystalline mesogens to be suitably stacked and positioned, thus forming into CLC with focal conic or polydomain texuture. When the mean surface charge density was greatly reduced and the repulsion couldn't block the strong hydrogen bonding affinity, the long-range ordered mesophases were completely collapsed and the iridescence originated from birefringence was almost lost as evidenced in Figure 1d and Figure 9f. Based on the schematic picture, the electrostatic repulsion resulted from surface charge and the helix nature of cellulose played vital roles in building up structure-color of hierarchical organizations of CNCs.

CONCLUSION

CNCs prepared by sulfuric acid hydrolysis retained the helicoids or handness character of cellulose chains, but blocked the hydrogen bonding affinity by

electrostatic repulsion originated from negative surface charge. Sonication treatment was an effective way to generate sub-scale leveled crystals with diminishing surface charge density, thus leading to the increment of the cholesteric pitch and the maximum reflective wavelength with increasing input sonication energy. The structure-color of CNC films followed the regulation of Bragg reflection (birefringence) and thin-film interference. There is a deviation from the linear relationship between pitch and wavelength since high input energy drove poly-domain hierarchical mesogens instead of planar phase arranged in the iridescent films. As a result, the structure-color of CNCs was controlled by the electrostatic repulsion; and the exact mechanism was thought to be applicable for many other polysaccharide nanocrystals. In order to obtain a uniform iridescent CNC film, short-range positional order and long-range orientation should take synergic effects. However, the chiral nematic transition during the solidification process was not clear yet and needed to be addressed in the future work.

ACKNOWLEDGEMENTS

The authors are grateful to National Natural Science Foundation of China (No. 51103073 & 21277073), Natural Science Foundation of Jiangsu Province (No. BK2011828), Scientific Research Foundation for the Returned Overseas Chinese Scholars, and Qing Lan Project and Six Talented Peak Program of Jiangsu Province and the Priority Academic Program Development of Jiangsu Higher Education Institutions for financial support.

REFERENCE

(1) Grunert, M.; Winter, W. T. Nanocomposites of Cellulose Acetate Butyrate Reinforced with Cellulose Nanocrystals. J. Polym. Environ. 2002, 10, 27-30.

(2) Shafiei-Sabet, S.; Hamad, W. Y.; Hatzikiriakos S. G. Rheology of Nanocrystalline Cellulose Aqueous Suspensions. Langmuir 2012, 28, 17124-17133.

(3) Habibi, Y.; Chanzy, H.; Vignon, M. R. TEMPO-mediated Surface Oxidation of Cellulose Whiskers. Cellulose 2006, 13, 679-687.

(4) Song, H.; Zhang, J.; Niu, Y.; Wang, Z. Phase Transition and Rheological Behaviors of Concentrated Cellulose/ionic Liquid Solutions. J. Phys. Chem. B 2010, 114, 6006-6013.

(5) Nickerson, R. F.; Habrle, J. A. Cellulose Intercrystalline Structure. Ind. Eng. Chem. 1947, 39, 1507-1512.

(6) Araki, J.; Wada, M.; Kuga, S.; Okano, T. Influence of Surface Charge on Viscosity Behavior of Cellulose Microcrystal Suspension. J. Wood Sci. 1999, 45, 258-261.

(7) Candanedo, S. B.; Roman, M.; Gray, D. G. Effect of Conditions on the Properties and Behavior of Wood Cellulose Nanocrystal Suspension. Biomacromolecules 2005, 6, 1048-1054.

(8) Ranby, B.G. Aqueous Colloidal Solutions of Cellulose Micelles. Acta Chem. Scand. 1949, 3, 649-650.

(9) Marchessault, R. H.; Morehead, F. F.; Koch, M. J. Some Hydrodynamic Properties of Neutral Suspensions of Cellulose Crystallites as Related to Size and Shape. J. Colloid Sci. 1961, 16, 327-344.

(10) Revol, J. F.; Godbout, L.; Dong, X. M.; Gray, D. G. Chiral Nematic Suspensions of Cellulose Crystallites: Phase Separation and Magnetic Field Orientation. Liq. Cryst. 1994, 16, 127-134.

(11) Urena-Benavides, E. E.; Ao, G.; Davis, V. A.; Kitchens, C. L. Rheology and Phase Behavior of Lyotropic Cellulose Nanocrystal Suspensions. Macromolecules 2011, 44, 8990-8998.

(12) Cranston, E. D.; Gray, D. G. Morphological and Optical Characterization of Polyelectrolyte Multilayers Incorporating Nanocrystalline Cellulose. Biomacromolecules 2006, 7, 2522-2530.

(13) Qi, H.; Shopsowitz, K. E.; Hamad, W. Y.; MacLachlan, M. J. Chiral Nematic Assemblies of Silver Nanoparticles in Mesoporous Silica Thin Films. J. Am. Chem. Soc. 2011, 133, 3728-3731.

(14) Shopsowitz, K. E. Qi, H.; Hamad, W. Y.; MacLachlan, M. J. Free-standing Mesoporous Silica Films with Tunable Chiral Nematic Structures. Nature 2010, 468, 422-425.

(15) Shafiei-Sabet, S.; Hamad, W. Y.; Hatzikiriakos, S. G. Rheology of Nanocrystalline Cellulose Aqueous Suspensions. Langmuir 2012, 28, 17124-17133.

(16) Han, J.; Zhou, C.; Wu, Y.; Liu, F.; Wu, Q. Self-assembling Behavior of Cellulose Nanoparticles during Freeze-drying: Effect of Suspension Concentration, Particle Size, Crystal Structure, and Surface Charge. Biomacromolecules 2013, 14, 1529-1540.

(17) Liu, D.; Chang, P. R.; Chen, M.; Wu, Q. Chitosan Colloidal Suspension Composed of Mechanically Disassembled Nanofibers. J. Colloid Interface Sci. 2011,

354, 637-643.

(18) Liu, D.; Wu, Q.; Chen, H.; Chang, P. R. Transitional Properties of Starch Colloid with Particle Size Reduction from Micro-to Nanometer. J. Colloid Interface Sci. 2009, 339, 117-124.

(19) Liu, D.; Chen, X.; Yue, Y., Chen, M.; Wu, Q. Structure and Rheology of Nanocrystalline Cellulose. Carbohydr. Polym. 2011, 84, 316-322.

(20) Beck, S.; Bouchard, J.; Berry, R. Controlling the Reflection Wavelength of Iridescent Solid Films of Nanocrystalline Cellulose. Biomacromolecules 2011, 12, 167-172.

(21) Ravi Kumar, M. N. V.; Bakowsky, U.; Lehr, C. M. Preparation and Characterization of Cationic PLGA Nanospheres as DNA Carriers. Biomaterials 2004, 25, 1771-1777.

(22) Feng, S.; Huang, G. Effects of Emulsifiers on the Controlled Release of Paclitaxel (Taxol) from Nanospheres of Biodegradable Polymers. J. Control Release 2001, 71, 53-69.

(23) Dong, X. M. Gray, D. G. Induced Phase Separation in Cellulose Nanocrystal Suspensions Containing Ionic Dye Species. Langmuir 1997, 13, 2404-2409.

(24) Dong, X. M.; Revol, J. F.; Gray, D. G. Effect of Microcrystallite Preparation Conditions on the Formation of Colloid Crystals of Cellulose. Cellulose 1998, 5, 19-32.

(25) Majoinen, J.; Kontturi, E.; Ikkala, O., Gray, D. G. SEM Imaging of Chiral Nematic Films Cast From Cellulose Nanocrystal Suspensions. Cellulose 2012, 19,

1599-1605.

(26) Kinoshita, S.; Yoshioka, S.; Miyazaki, J. Physics of Structural Colors. Rep. Prog. Phys. 2008, 71, 076401.

(27) de Vries, H. Rotatory Power and Other Optical Properties of Certain Liquid Crystals. Acta Crystallogr. 1951, 4, 219-226.

(28) Chilaya, G. S.; Lisetski, L. N. Cholesteric Liquid Crystals: Physical Properties and Molecular-statistical Theories. Mol. Cryst. Liq. Cryst. 1986, 140, 243-286.

(29) Neville, A. C. Biology of Fibrous Composites; Development beyond the Cell Membrane. Cambridge: The University Press. 1993

(30) Marchessault, R. H.; Morehead, F. F.; Walter, N. M. Liquid Crystal Systems From Fibrillar Polysaccharides. Nature 1959, 184, 632-633.

(31) Revol, J. F.; Bradford, H.; Giasson, J.; Marchessault, R. H.; Gray, D. G. Helicoidal Self-Ordering of Cellulose Microfibrils in Aqueous Suspension. Int. J. Biol. Macromol. 1992, 14, 170-172.

(32) Viswanathan, A.; Shenouda, S. G. The Helical Structure of Cellulose I. J. Appl. Polym. Sci. 1971, 15, 519-535.

(33) Nishiyama,Y.; Sugiyama, J.; Chanzy, H.; Langan, P. Crystal Structure and Hydrogen Bonding System in Cellulose Iα From Synchrotron X-ray and Neutron Fiber Diffraction. J. Am. Chem. Soc. 2003, 125, 14300-14306.

(34) Hou, H.; Reuning, A.; Wendorff, J. H.; Greiner, A. Tuning of the Pitch Height of Thermotropic Cellulose Esters. Macromol. Chem. Phys. 2000, 201, 2050-2054.

(35) Chilaya, G. Induction of Chirality in Nematic Phases. Revue Phys. Appl. 1981, 16, 193-208.

Table 1. Parameters of CNC in the Suspension or in Solidified Cholesteric Liquid Crystal Film with Different Sonication Times. (Zeta-potential, Z-average size, and PDI were measured by Zeta-sizer; length or diameter of CNC were measured by AFM; and pitch or wavelength at peak was measured by POM and UV-Vis, respectively.)

Sonication time (min)	Zeta potential (mV)	Z-average size (nm)	PDI	Length of CNC (nm)	Diameter of CNC (nm)	Surface charge density (e/nm^2)	Half pitch (μm)	Maximum reflection wavelength (nm)
0	-50.6 ± 0.2	176.2	0.427	159 ± 8	50 ± 2	0.67	0.554	328.46
10	-51.0 ± 0.5	95.6	0.519	122 ± 15	38 ± 4	0.51	0.756	442.03
20	-52.2 ± 0.2	76.2	0.517	120 ± 18	36 ± 5	0.48	0.877	507.25
30	-52.7 ± 0.3	74.1	0.501	119 ± 20	35 ± 5	0.47	0.965	538.66
40	-53.0 ± 0.3	73.1	0.481	114 ± 19	34 ± 6	0.45	1.010	550.73
50	-53.6 ± 0.4	69.1	0.490	106 ± 24	33 ± 7	0.44	1.068	594.22
60	-54.0 ± 0.3	68.7	0.496	87 ± 25	30 ± 6	0.39	1.205	664.31
70	-54.1 ± 0.4	67.7	0.549	81 ± 28	28 ± 8	0.37	1.260	671.57

Scheme 1. Cholesteric Phase Transition of CNCs Induced by Inputing Sonication Energy.

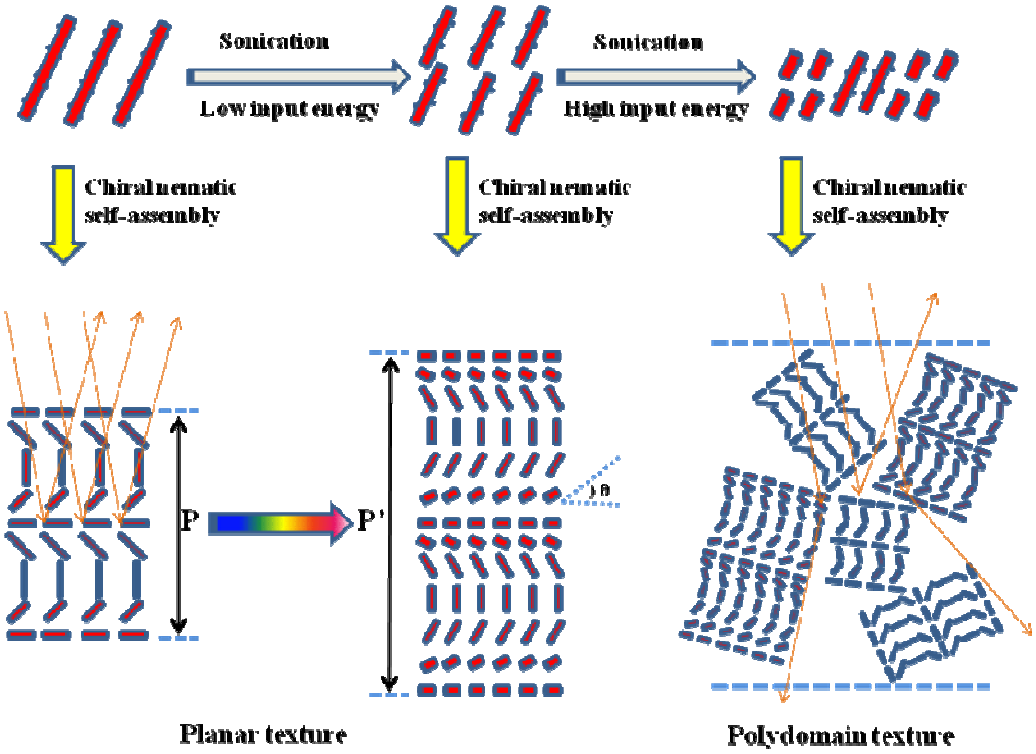

Figure captions

Figure 1. (a) AFM micrographs of fresh-prepared CNCs and (b) CNCs sonicated for 70 min , and the corresponding statistical distribution of particle length (c and d).

Figure 2. POM photographs of CNC films processed at (a) 30 ^{o}C, (b) 45 ^{o}C, (c) 50 ^{o}C and (d) 70 ^{o}C, respectively. (sonication at 300 W for 10 min)

Figure 3. Reflection spectra (90º incidence and detection angles) of CNC films with thickness of 42, 63, 82, 96 μm. (sonication at 300 W for 30 min and casting at 30 ^{o}C).

Figure 4. Photographs of CNC films cast from the suspensions sonicated for (a) 0, (b) 10, (c) 20, (d) 30, (e) 40, and (f) 50 min, respectively.

Figure 5. Reflection spectra (90º detection angle) of CNC films cast from the suspensions sonicated for 0, 10, 20, 30, 40, 50, 60, and 70 min, respectively. (Thickness of the films is 96 μm)

Figure 6. POM micrographs of CNC films cast from the suspensions sonicated for (a) 0, (b)10, (c) 20, (d) 30, (e) 40, (f) 50, (g) 60, and (h) 70 min , respectively.

Figure 7. Dependence of the maximumreflective wavelength on the cholesteric pitch of CNC films.

Figure 8. Reflection spectra (90º detection angle) of CNC films cast from the suspensions sonicated at 520 W for 10, 30, and 120 min. (The inset shows photographs of solidified CNC films under corresponding sonication treatment. Thickness of the films is 96 μm.)

Figure 9. POM images of CNC films cast from the suspensions sonicated at 520 W for (a and b) 10, (c and d) 60, (e) 120, and (f) 150 min, respectively.

Figure 10. SEM micrographs of the cross-section of CNC films cast from the suspensions sonicated for (a) 0, (b) 10, (c) 30, (d) 50, (e) 60, (f) 70 min, respectively. (The inset of 10b shows high resolution micrograph of solidified CNC films.)

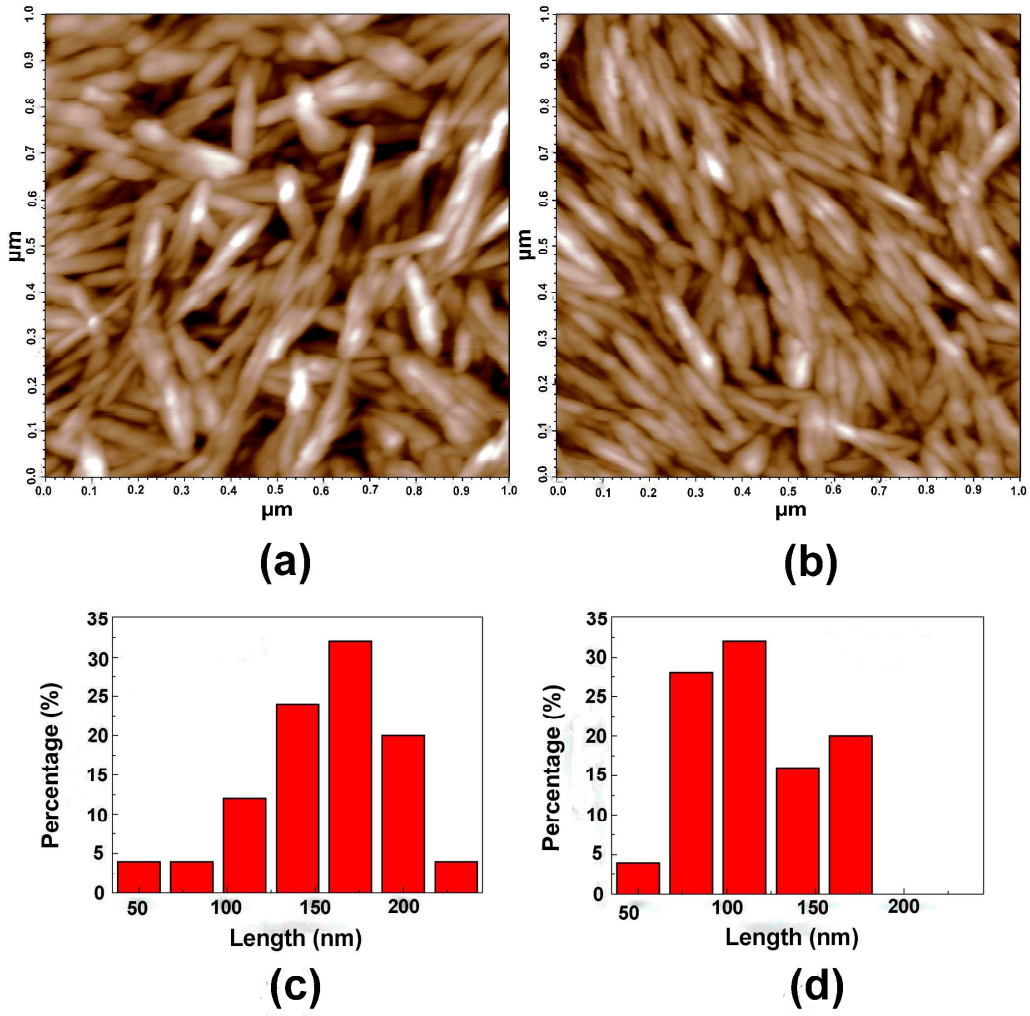

Figure 1. (a) AFM micrographs of fresh-prepared CNCs and (b) CNCs sonicated for 70 min, and (c and d) the corresponding statistical distribution of particle length .

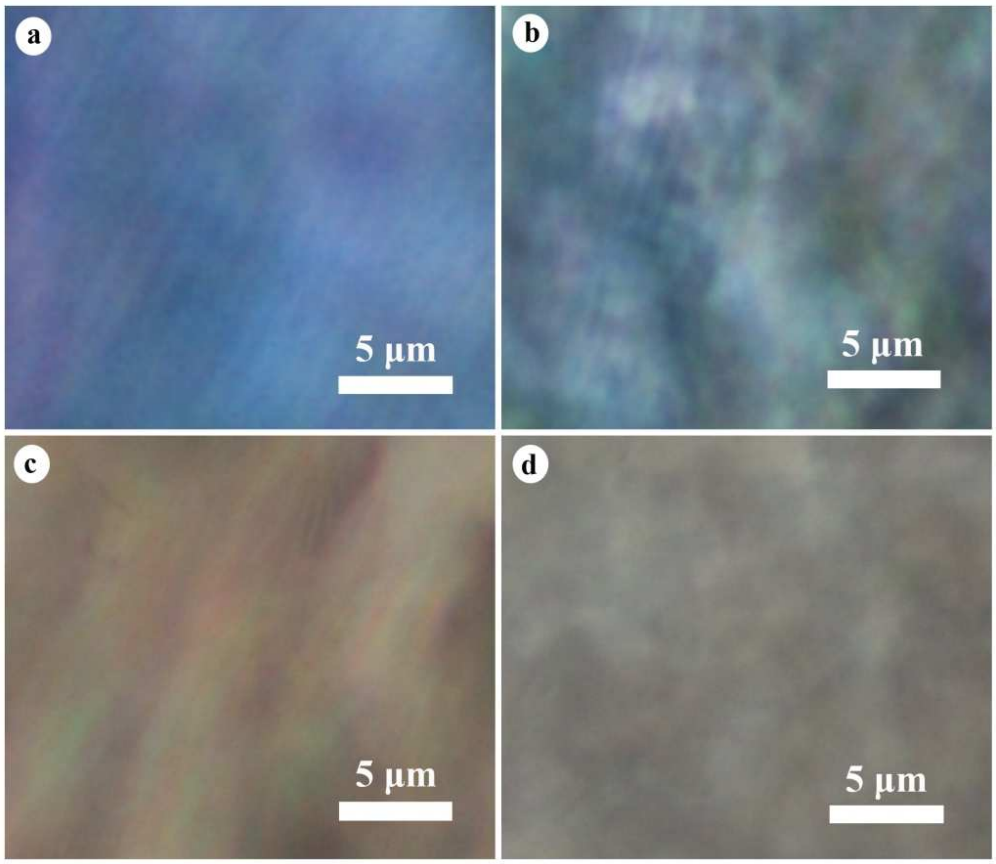

Figure 2. POM photographs of CNC films processed at (a) 30 ^{o}C, (b) 45 ^{o}C, (c) 50 ^{o}C and (d) 70 ^{o}C, respectively. (sonication at 300 W for 10 min)

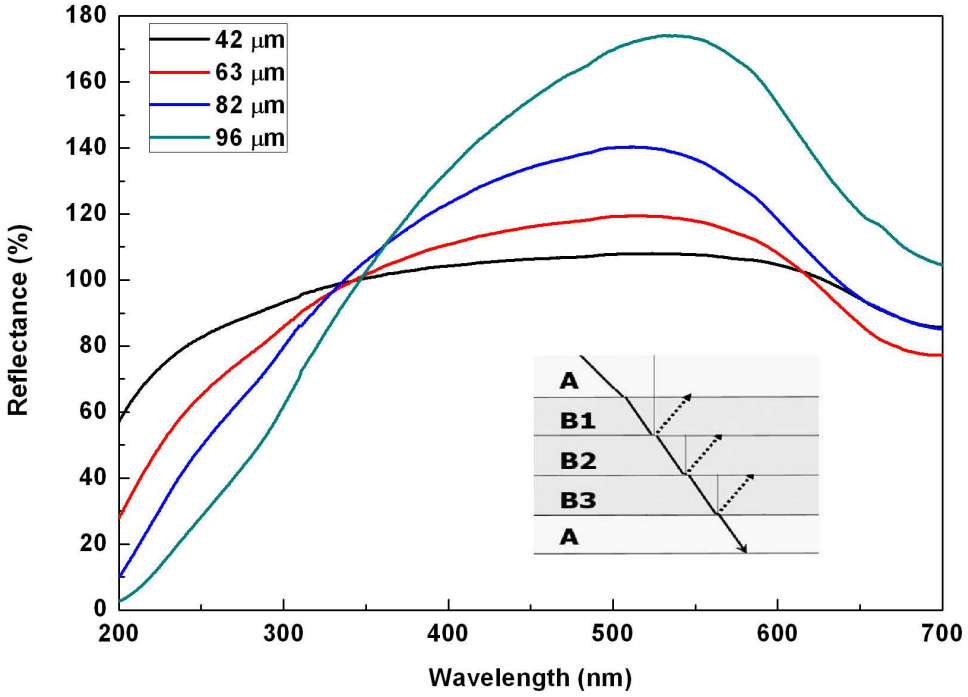

Figure 3. Reflection spectra (90º incidence and detection angles) of CNC films with thickness of 42, 63, 82, 96 μm. (sonication at 300 W for 30 min and casting at 30 ^{o}C).

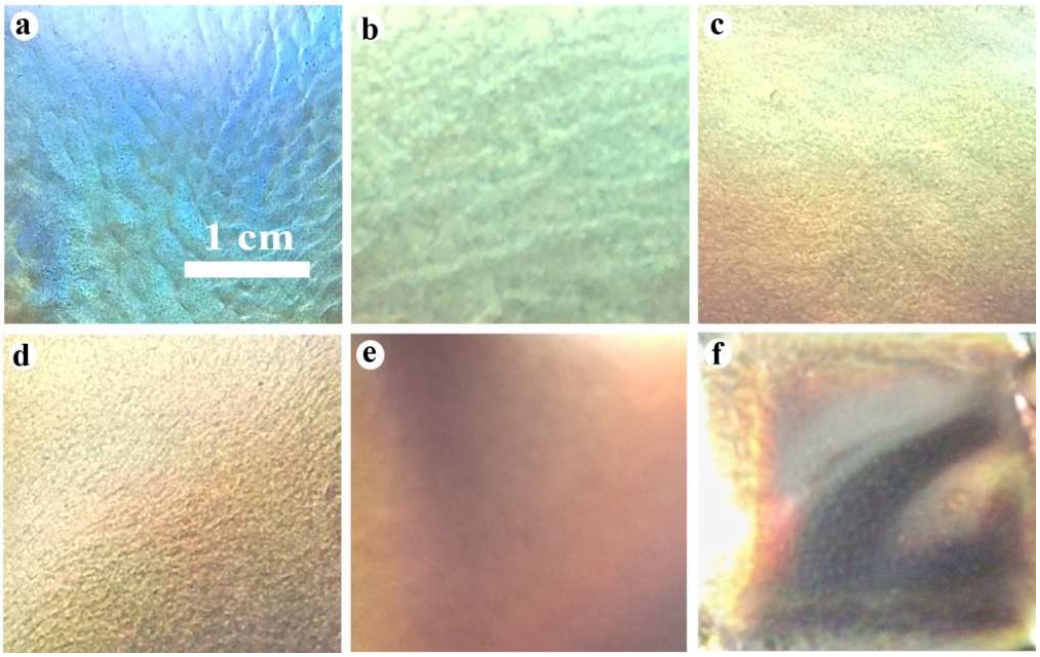

Figure 4. Photographs of CNC films cast from the suspensions sonicated for (a) 0, (b) 10, (c) 20, (d) 30, (e) 40, and (f) 50 min, respectively.

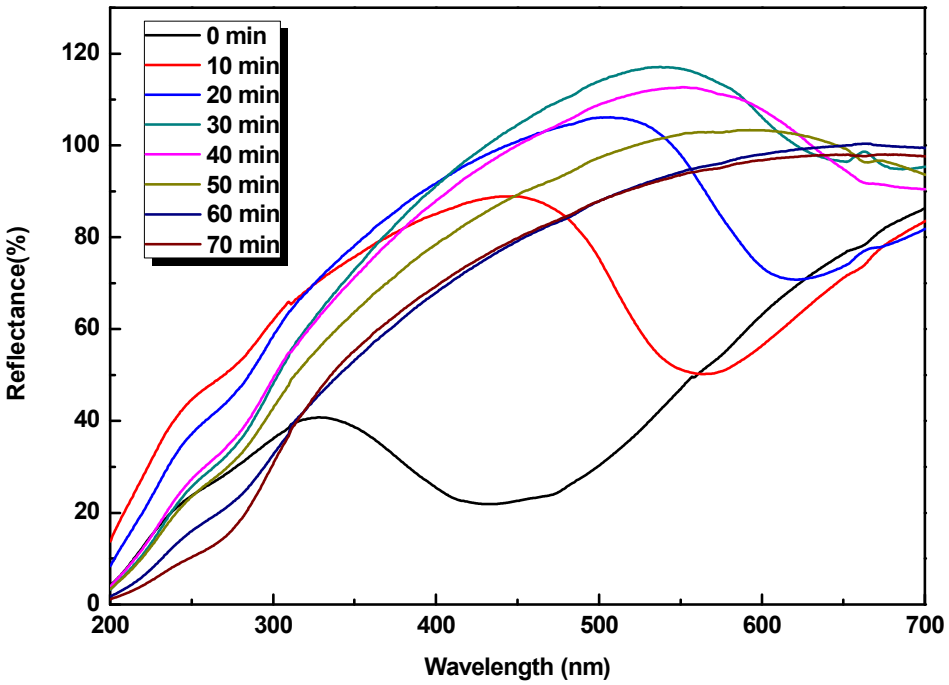

Figure 5. Reflection spectra (90º detection angle) of CNC films cast from the suspensions sonicated for 0, 10, 20, 30, 40, 50, 60, and 70 min, respectively. (Thickness of the films is 96 μm)

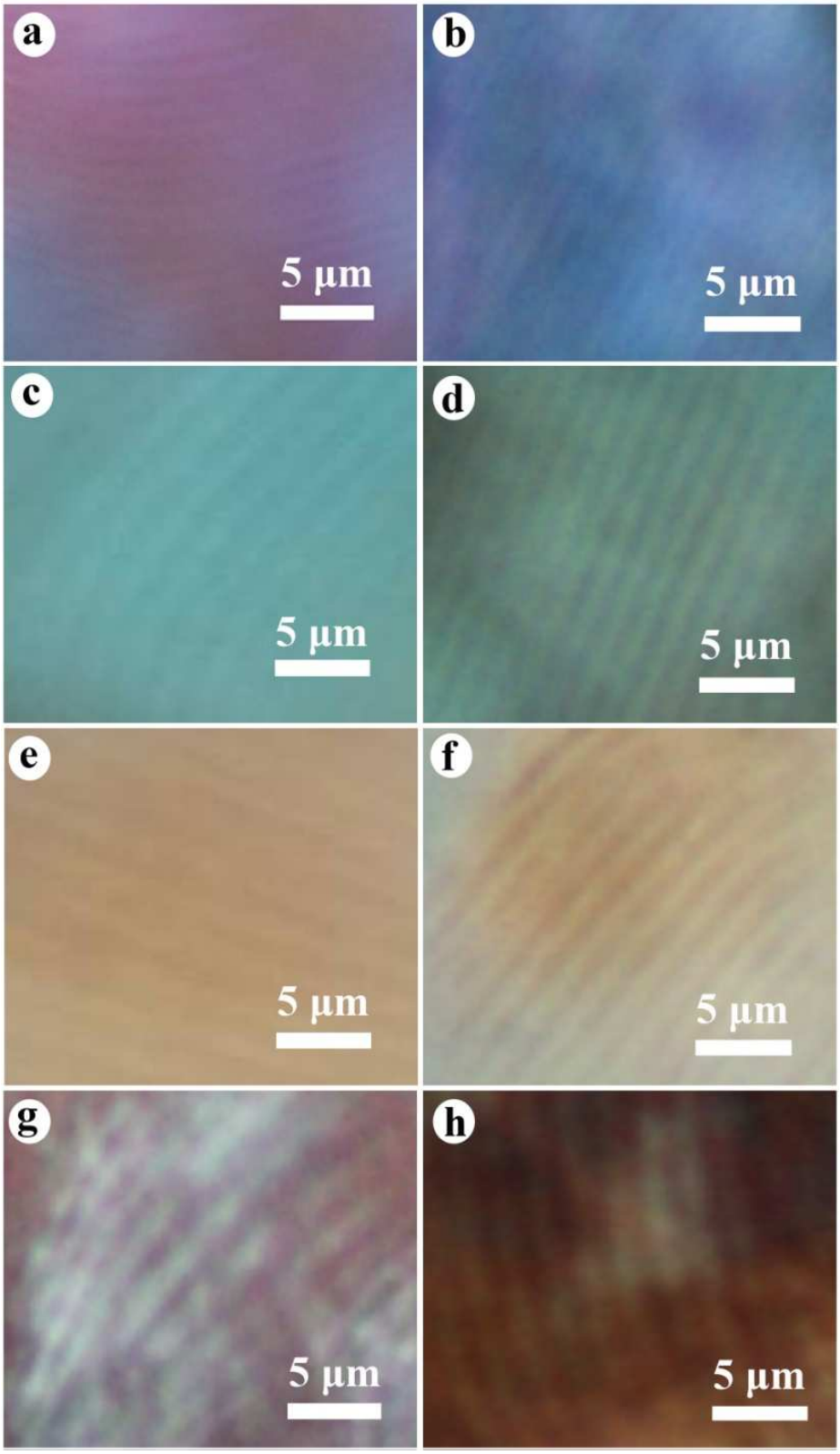

Figure 6. POM micrographs of CNC films cast from the suspensions sonicated for (a) 0, (b) 10, (c) 20, (d) 30, (e) 40, (f) 50, (g) 60, and (h) 70 min, respectively.

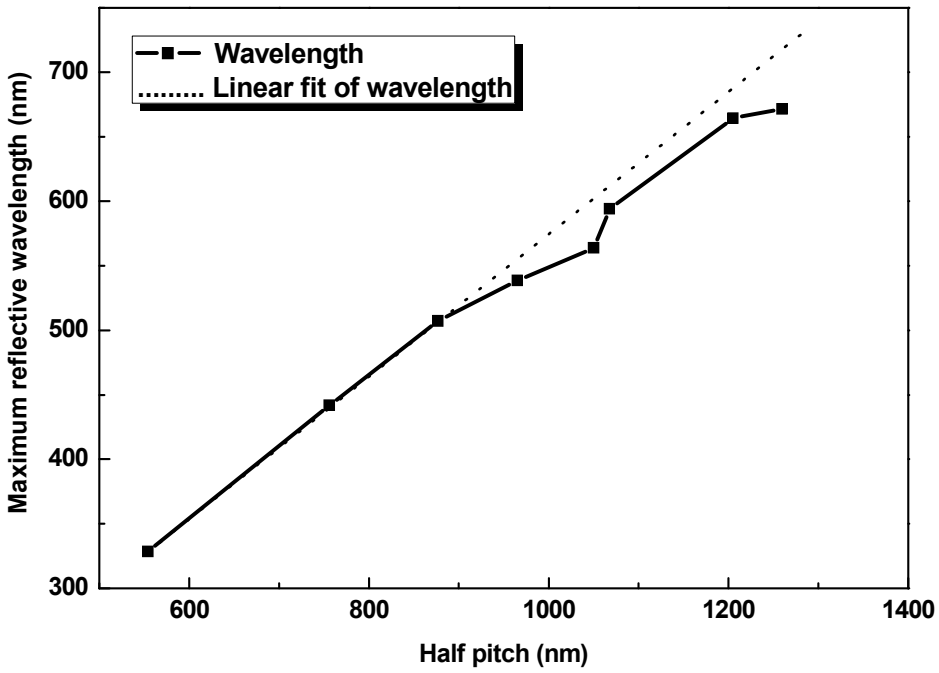

Figure 7. Dependence of the maximum reflective wavelength on the cholesteric pitch of CNC films.

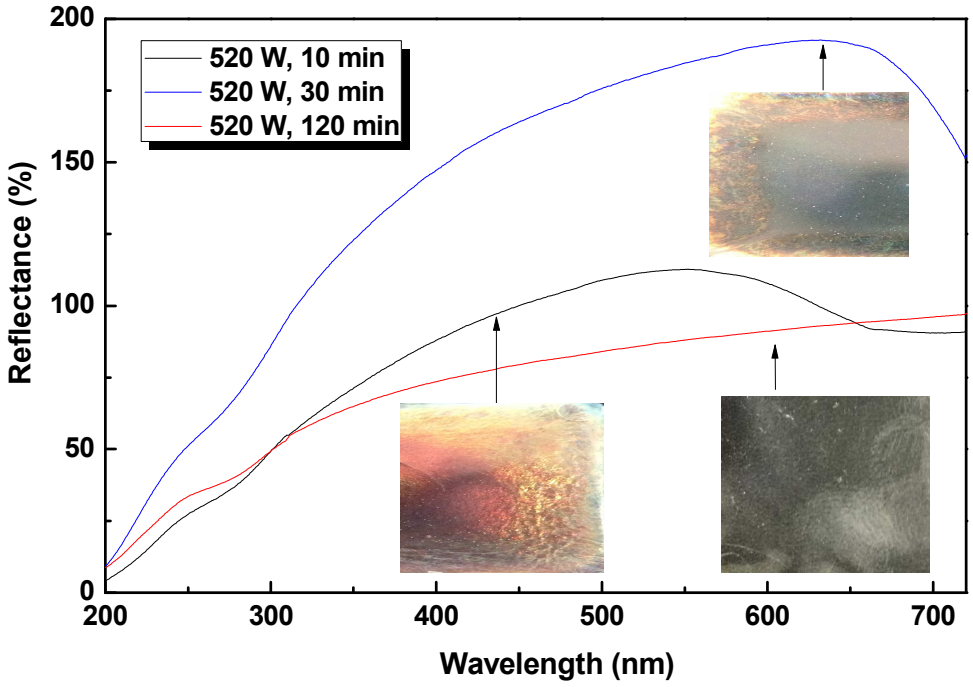

Figure 8. Reflection spectra (90º detection angle) of CNC films cast from the suspensions sonicated at 520 W for 10, 30, and 120 min. (The inset shows photographs of solidified CNC films under corresponding sonication treatment. Thickness of the films is 96 μm.)

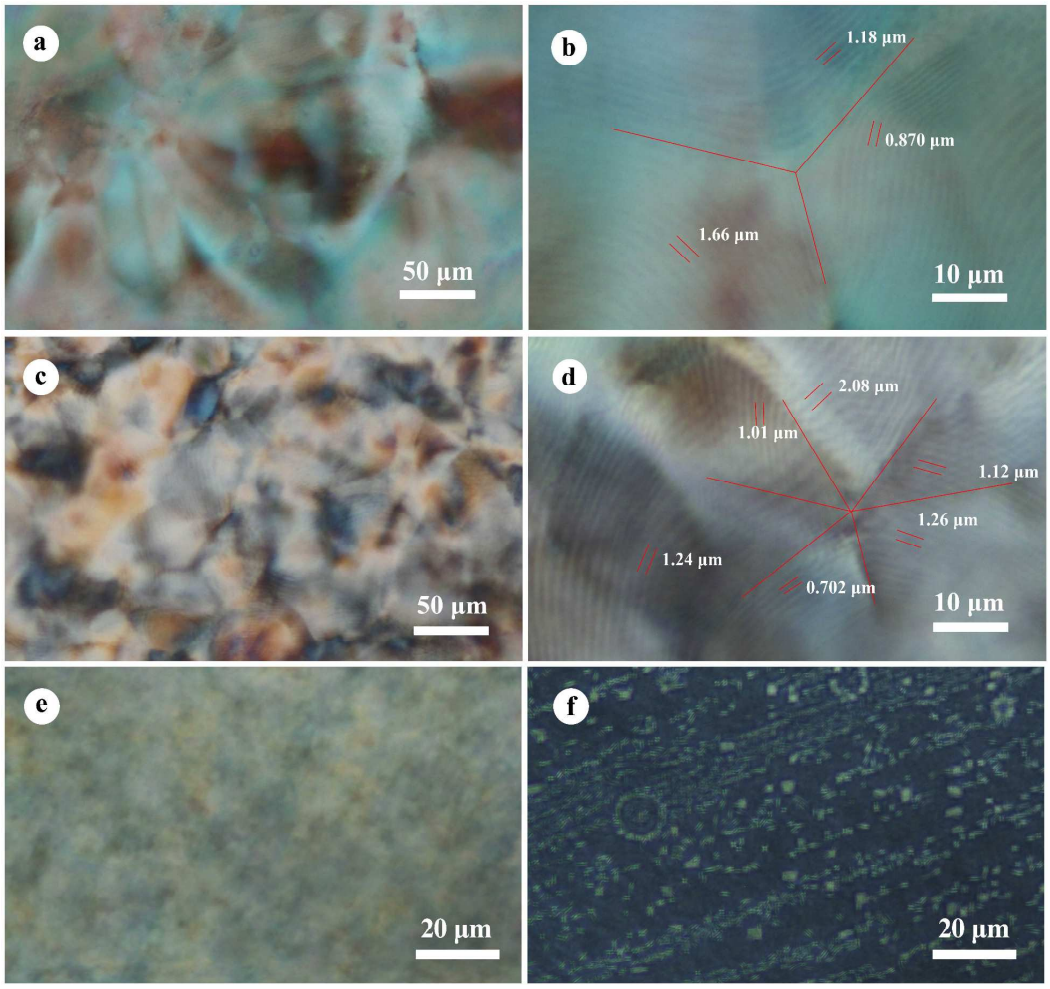

Figure 9. POM images of CNC films cast from the suspensions sonicated at 520 W for (a and b) 10, (c and d) 60, (e) 120, and (f) 150 min, respectively.

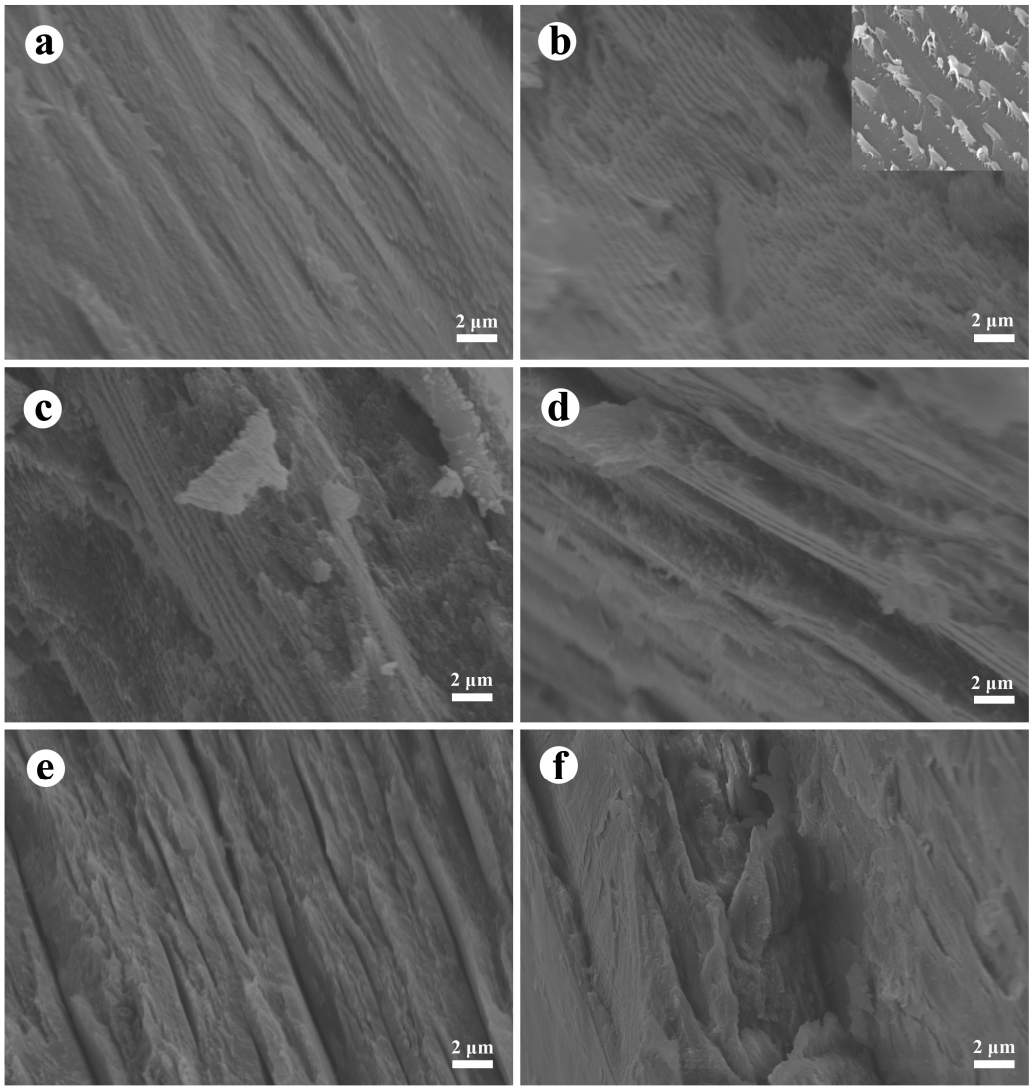

Figure 10. SEM micrographs of the cross-section of CNC films cast from the suspensions sonicated for (a) 0, (b) 10, (c) 30, (d) 50, (e) 60, (f) 70 min, respectively. (The inset of 10b shows high resolution micrograph of solidified CNC films.)